This document is the Preprint version of a Published Work that appeared in final form in Computers & Geosciences 122 : 113-119 (2019), copyright © 2018 Elsevier. To access the final edited and published work see https://doi.org/10.1016/j.cageo.2018.10.007

Analysis of atmospheric thermodynamics using the R package aiRthermo

Jon Sáenz[a,b,*], Santos J. González-Rojí[a], Sheila Carreno-Madinabeitia[c,a], Gabriel Ibarra-Berastegi[d,b]

[a] *Dept. Applied Physics II, Universidad del País Vasco-Euskal Herriko Unibertsitatea (UPV/EHU), Barrio Sarriena s/n, 48940-Leioa, Spain*

[b] *BEGIK Joint Unit IEO-UPV/EHU, Plentziako Itsas Estazioa (PIE, UPV/EHU), Areatza Pasealekua, 48620 Plentzia, Spain*

[c] *Meteorology Area, Energy and Environment Division, TECNALIA R&I, Basque Country, Spain.*

[d] *Dept. Nuc. Eng. and Fluid Mech., Universidad del País Vasco-Euskal Herriko Unibertsitatea (UPV/EHU), Alameda Urquijo s/n, 48013-Bilbao, Spain.*

Abstract

The publicly available R package *aiRthermo* is presented in this study, which allows the user to process information relative to atmospheric thermodynamics, ranging from calculating the density of dry or moist air and converting data between moisture indices to processing a full sounding, obtaining factors such as the convective available potential energy, additional instability indices, or adiabatic evolutions of particles. The package also provides the possibility to present information using customisable Stüve diagrams. Many of the functions are written inside a C extension to ensure that the computations are fast. The results of applying this package to five years of real soundings measured over the Iberian Peninsula are also presented as an example. The package considerably extends the capabilities of R to process atmospheric soundings or model results. This will be useful for many practical environmental forecasting applications at different scales, such as statistical downscaling for climate analysis, quantitative precipitation forecasting (particularly precipitation extremes), diagnosing storms, flash floods, and lightning, and in aviation and other fields where computing atmospheric convection and its related parameters is important.

*Corresponding author: Jon Sáenz

Email addresses: `jon.saenz@ehu.eus` (Jon Sáenz), `santosjose.gonzalez@ehu.eus` (Santos J. González-Rojí), `sheila.carreno@tecnalia.com` (Sheila Carreno-Madinabeitia), `gabriel.ibarra@ehu.eus` (Gabriel Ibarra-Berastegi)

URL: `http://www.ehu.eus/eolo` (Jon Sáenz)

Authorship statement: Jon Sáenz thought up the original concept of the package, wrote most parts of the C code, several parts of the R code, and some of the verification

Keywords: atmospheric thermodynamics, adiabatic evolution, instability indices, Stüve diagram, CRAN, R package

routines. He was also the lead author of the paper. Santos J. González-Rojí wrote some parts of the R and verification codes, packaged the software for its inclusion in CRAN, and wrote some parts of the paper. Sheila Carreno-Madinabeitia was the author of the Stüve plotting routines and parts of the verification code. She analysed the sounding database presented in the paper and participated in the writing. Gabriel-Ibarra Berastegi was involved in the verification of results, the testing of the package, and the writing of the paper.

Declarations of interest:

The only interest of the authors is to make the package known. If the paper is accepted, their scientific merit will also be publicly recognised.

Highlights

1. A new R-package providing new functions in atmospheric thermodynamics is presented.
2. The package provides analyses and Stve diagrams not previously available in R.
3. A case-study (2010-2014) of soundings over the Iberian Peninsula is presented.
4. The package can play a key role in advanced forecast and diagnostic systems.
5. The most critical functions are written in C to speed up computation.

1. Introduction

R (`https://www.cran.r-project.org/`) is a freely available software for statistical computing that has expanded exponentially in recent years. Some packages at the intersection between air pollution, climate, and atmospheric studies make R a powerful tool for processing data and visualising atmospheric processes, such as air pollution [1] and hydrology [2], and mapping [3] processing satellite [4] and atmospheric data [5]. Additional useful packages in this field, such as *RAtmosphere*, *ClimDown*, *opentraj*, and others, can be downloaded from the CRAN repository.

However, the analysis of atmospheric soundings and water vapour from the perspective of atmospheric thermodynamics is an area where the community of atmospheric scientists have new needs using R, as identified by the authors. *aiRthermo* extends the functionality offered by the *RadioSonde* and *meteogRam* packages by adding Stüve diagrams and the vertical evolution of air parcels.

Under the typical pressure and temperature conditions found in the atmosphere, the state of dry air is commonly described by two thermodynamic variables (pressure P and temperature T). The concentration of water can be expressed using different moisture indices, such as the specific humidity, mixing ratio, virtual temperature, and relative humidity. Phase changes of water cause large latent heat fluxes that must be considered as air parcels ascend or descend [6, 7, 8] when studying atmospheric stability and convection.

Some instability indices are often used when diagnosing meteorological situations. For example, the relationship between sea breeze and precipitation over Hainan Island [9], the role of moist convection in the development of flash floods [10], or the retrieval of precipitation in the Tropical Rainfall Measuring Mission (TRMM) mission [11], to name a few. Thermodynamic variables and indices are also used for the statistical downscaling of extreme precipitation events and moisture transport [12].

The main objective of this paper is to present an R package that has been designed to allow scientists to conduct computations involving atmospheric thermodynamics using the R language. This considerably extends the capabilities of R for meteorological data analysis, and has, for instance, allowed us to extend the lectures offered at the M.Sc. level [13], enabling students to perform numerical exercises involving with these parameters.

2. Data

2.1. Sample data provided with the package

The data used in Section 4 of this paper (provided in the package for testing by users) were collected from a server located at the University of Wyoming (publicly available at `http://weather.uwyo.edu/upperair/sounding.html`). The first sounding used in this paper (sounding A) was measured at Santander, Spain (station ID 08023, date 2010-06-16, 12:00 UTC), and corresponds to a day that faced some frontal rain. The second case (sounding D) was measured at Barcelona, Spain (station ID 08190, 2013-08-07, 12:00 UTC) and reflects a situation with substantial convective instability. The final example (Davenport, USA, station ID 74455, 1997-06-21 at 00 UTC) is also used to illustrate a case with strong convection [14].

2.2. Data for the case study

The topography of the Iberian Peninsula and the positions of the eight sounding sites are shown in Figure 1. The sounding files downloaded from Wyoming University's server covered the period of 2010-2014. The number of cases depends on the site, and ranges from 1705 over Lisbon to 3575 over Murcia. The instability index values computed at Wyoming University and those computed using the functions in *aiRthermo* were compared. In *aiRthermo*, the initial conditions for CAPE were obtained by vertically averaging the lowest 500 m of the sounding and by performing isobaric precooling for the resulting low-level average particle values.

3. Methodology

Most of the theory and methods used to develop *aiRthermo* can be found in standard references [6, 7, 8, 14, 15]. However, some of our assumptions are documented below.

The state of an air parcel is defined in *aiRthermo* using its pressure P (Pa), temperature T (K), and mixing ratio w (kg kg^{-1}). To compute the saturation

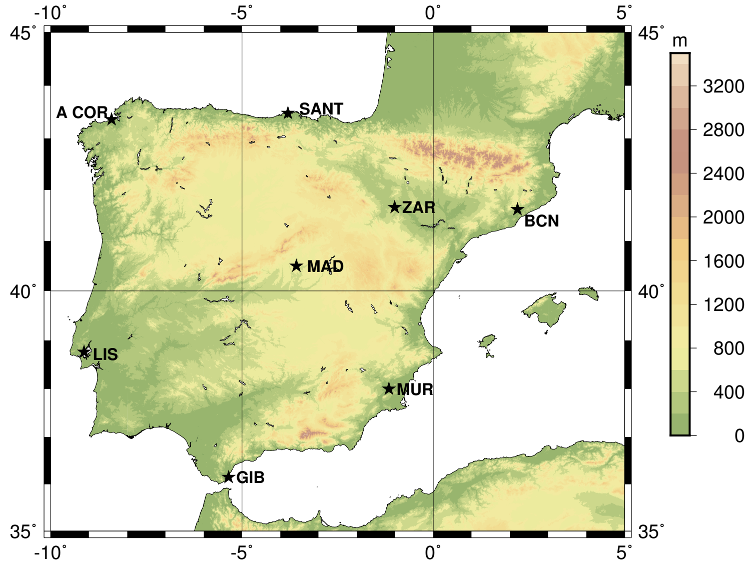

Figure 1: Map of the Iberian Peninsula showing the stations where soundings are routinely measured.

pressure of water over a flat surface, we follow the expressions on pages 197-200 from [6] for ice and water below 30°C, and Buck's equation [16] above 30°C. The dew-point temperature is given by the approximate expression of 5.68 in [6] from the given P and mixing ratio w.

The specific heat of moist air at a constant pressure and volume are computed as $c_{pm} = c_{pd}\,(1 + 0.87q)$ and $c_{vm} = c_{vd}\,(1 + 0.97q)$, following [14], with $c_{pd} = 1005$ J kg^{-1} K^{-1} and $c_{vd} = 718$ J kg^{-1} K^{-1} [6, 7]. By default, the functions that provide these specific heats will return the values corresponding to moist air, and values corresponding to dry air can be requested by explicitly building a dry air parcel.

A good analytical expression for the latent heat of evaporation of water does not exist, therefore, an approximate expression is used. For liquid water ($T \in [233.15, 313.15]$ K interval), we use cubic polynomial expansion based on tabulated values [15] with an absolute residual smaller than 1 J kg^{-1}, and all terms are statistically significant at the 99% confidence level. By doing this, we assume that super-cooled water can exist up to the Schaefer point (about -40°C). The result for ice is based on a quadratic fit to the observed values [17] in the interval of $T \in [210, 273.15]$ K (residuals smaller than 0.05 J kg^{-1}). As the values corresponding to water and ice differ in the common interval used in the previous two expressions, a linear combination of ice's (L_i) and water's (L_w) latent heat is computed $L = w_i L_i + (1 - w_i) L_w$ with a weight of $w_i = 1 - \frac{T-253.15}{20}$ in the interval of $T \in [253.15, 273.15]$ K. Below 253.15 K, the latent heat corresponding to ice is applied, and that corresponding to water is used above 273.15 K.

All vertical evolutions are computed assuming that a hydrostatic balance is in place. Therefore, $\Gamma_d^* = \left(\frac{dT}{dP}\right)_d = \frac{\Gamma_d}{\rho g}$ and $\Gamma_s^* = \frac{\Gamma_s}{\rho g}$ are used, with Γ_d and Γ_s as the typical expression for vertical gradients in Z. For the saturated pseudoadiabatic profile, the expression used for the pressure coordinates is transformed from the common expression provided in z [6, 7, 8, 14]. Using the expressions of Γ_d^* (Γ_s^*) for dry (saturated) adiabatic evolutions, the vertical evolution of an air parcel from the initial state P_0, T_0, and w_0 is computed by numerically solving the ordinary differential equation $\frac{dT}{dP} = \Gamma_i^*(P, T, w)$, with $i = d$ or $i = s$ depending whether or not the particle is saturated. This differential equation is numerically solved using the fourth-order Runge-Kutta scheme for all vertical evolutions, with saturation checks at each vertical step.

For some of the indices, such as the Lifted Index (LI) or Convective Available Potential Energy (CAPE), it is customary to calculate the vertical average of the lower levels to identify a representative parcel P_0, T_0, w_0 of the lowest levels of the atmosphere [18, 19]. These vertical averages at low levels are evaluated in all cases by first considering

$$\Delta Z = \frac{R_d}{g} \int_{P_t}^{P_s} \frac{T_v dP}{P} \tag{1}$$

as the vertical width of the parcel. Next, the accumulated vertical quantity value $X(P)$ is given by

$$\bar{X} = \frac{1}{\Delta Z} \frac{R_d}{g} \int_{P_t}^{P_s} \frac{X k T_v}{P} dP \tag{2}$$

where $k(P)$ serves as a normalising function. When calculating the average temperature, $k(P) = 1$ is used. In contrast, the specific humidity $k(P) = q(P)$ is used to indicate moisture. The vertical integrals are computed using discrete slabs defined by the data given by the soundings in all cases. For these discrete slabs, the integrals are computed analytically and the results are accumulated.

To compute CAPE and convective inhibition (CIN), the vertical integrals are computed in pressure levels by adding the energy corresponding to discrete slabs defined by linear or logarithmic vertical profiles, which are defined by the soundings. The integrals for each of the slabs enclosed by linear profiles are computed analytically, and the energy corresponding to each slab is accumulated, producing the final value of CAPE or CIN. The integrals are always calculated using the virtual temperature [20].

There are different methods of accurately determining the lifting condensation level (LCL) or the equivalent potential temperature of an air parcel in *aiRthermo*. In the first case, the package calculates these variables by computing their vertical evolutions and numerically solving the ordinary differential equation representing their ascent from the initial conditions given by their temperature, pressure, and mixing ratio. For compatibility, functions that allow these variables from well-known alternative equations to be computed, such as the approximate method presented by Bolton [21] to compute LCL, are also provided.

The routine designed to produce Stüve diagrams for either the soundings or the lifted particles used in the computation of CAPE/CIN extends the available options for thermodynamic diagrams in the existing RadioSonde R package. The routine that plots the Stüve diagram uses the equivalent potential temperature lines, constant mixing ratio lines, or dry adiabatic lines produced by the routines in *aiRthermo* to ensure the full consistency of results. The routine that plots the Stüve diagram allows the user to plot additional lines in the sounding, enabling the production of highly customisable plots.

4. Description of the package

The package contains over 40 functions that can be separated into six large groups according to their functionality. A brief description of each set of functions is presented here, however, the manual of the package must be checked for a full description of the functions and the parameters required to run them. The manual can be found on the web-page for the package *aiRthermo* in the Comprehensive R Archive Network (CRAN).

- **Density of dry/moist air and virtual temperature**

  The density of air can be directly calculated using the corresponding function `densityMoistAir`, or by using intermediate functions to independently calculate the densities of dry air and water vapour (`densityDry` and `densityH2Ov`). The virtual temperature of an air parcel can also be directly calculated by using the `virtual_temperature` function.

- **Conversion of moisture indices**

  Several functions that allow conversion between moisture indices through the dew point temperature, mixing ratio, and specific or relative humidity are included in *aiRthermo*. The most important functions of this category are those converting the relative humidity to the mixing ratio (`rh2w`), the relative humidity to the specific humidity (`rh2shum`), the mixing ratio to the dew point temperature (`w2Td`), and the mixing ratio to the specific humidity or the reverse (`w2q` and `q2w`), or `e2w` that to convert the partial pressure of water vapour to the mixing ratio.

- **Saturation mixing ratios or pressures**

  This class includes all functions that use the Clausius-Clapeyron equation to calculate the saturation mixing ratios or pressures. The most important function is `saturation_pressure_H2O`, which computes the saturation pressure e_s in Pa as a function of the temperature. As well as this, `saturation_mixing_ratio` returns the saturation mixing ratio w_s in kg kg^{-1}.

- **State and evolution of an air parcel**

  The package calculates the internal state of a parcel using a given pressure, temperature, and mixing ratio with the function `parcelState`. However, to calculate the vertical evolution of an air parcel, *aiRthermo* determines the correct function depending on the state of the particle and the environment. General ascent from a given initial pressure to the final pressure is computed by the `adiabatic_ascent` function, which selects the type of evolution depending on the saturation of the parcel. Downwards evolution can also be computed using `AnyAdiabaticDown`, but it requires the initial amount of water available in the cloud for evaporation (in kg/kg). Conversions between the potential temperature, Temperature, and pressure can be calculated using `PT2Theta`, `PTheta2T`, and `TTheta2P`, which are useful if dry adiabatic processes are occurring.

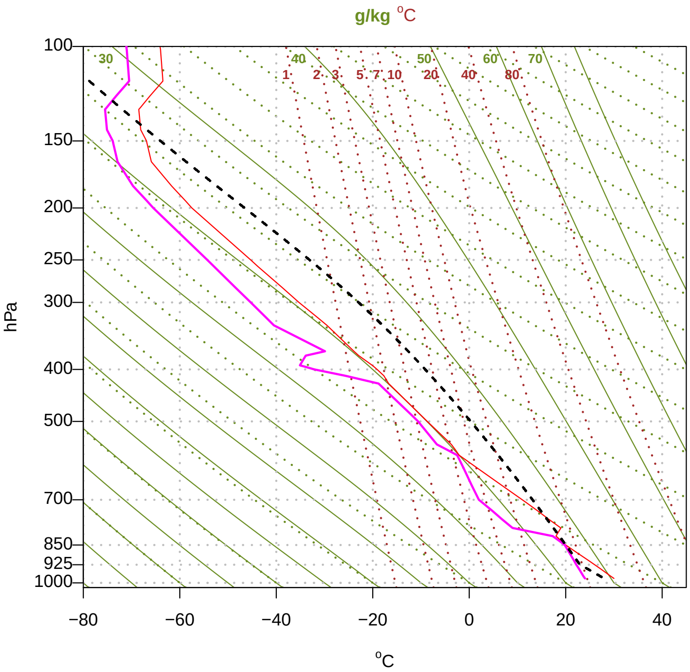

Figure 2: Example of a Stüve diagram plotted with *aiRthermo*. The temperature (red) and dew point temperature (magenta) of the sounding area are plotted together with the evolution of the lifted air parcel (shaded black line).

- **Instability indices**

  Several functions compute common instability indices such as K, the Total-Totals, the Showalter, and the LI indices (functions `Kindex`, `TTindex`, `Sindex`, and `LIindex`). `CAPE_CIN` calculates the values of CAPE and CIN, the LCL, the Level of Free Convection (LFC), the End Level (EL), and the trajectory, followed by the lifted parcel. The *PlowTop* argument provides the width of a slab across which a vertical average will be taken through the bottom of the sounding to obtain the initial conditions of the ascending parcel. *precoolType* determines the type of precooling that must be applied to the initial parcel. *upToTop* controls whether the lifted particle continues upwards after it first crosses the ambient sounding.

- **Stüve diagrams**

  The `stuve_diagram` function is included to allow the creation of high-

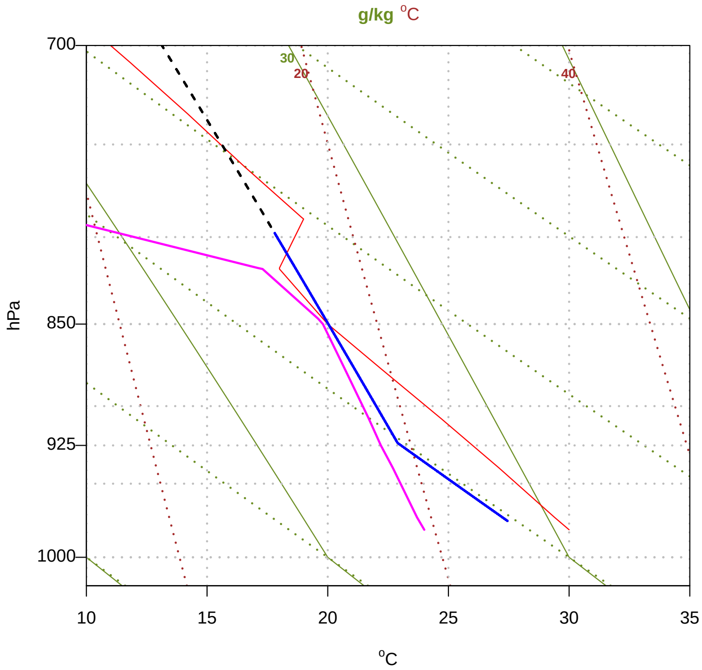

Figure 3: Detail of the example Stüve diagram in Figure 2 magnifying its lower levels to show the different evolutions of the lifted parcel depending on the value of the *upToTop* parameter (*TRUE* (black line) and *FALSE* (blue line)).

quality Stüve diagrams. As well as generating the Stüve diagram, they can also represent the trajectory followed by any ascending air parcel (when `CAPE_CIN` is called using *getLiftedBack=TRUE*).

Figure 2 shows the Stüve diagram corresponding to the Davenport sample sounding. Major differences in the estimated CAPE for the sounding can appear if the *upToTop* attribute is set to *TRUE* or *FALSE* (discontinuous black and blue lines in Figure 3 respectively) as the lifting particle slightly crosses the sounding at low levels. These results can be controlled using the appropriate parameters. Sensible default parameters are used by the function if they are not explicitly provided by the user.

Listing 1 shows the manner in which `CAPE_CIN` can be used to produce a figure similar to Figure 2. Each time `CAPE_CIN` is called, `getLiftedBack` can be set to *TRUE* so that the trajectory of the lifted parcel is returned to the calling environment. The discontinuous black line in Figure 2 shows the trajectory of the ascending parcel when it is requested to ascend to the top of the sounding (*upToTop=TRUE*). If *FALSE* is assigned to the upToTop parameter, the parcel (blue line in Figure 3) stops after the first time that the ascending parcel is not buoyant, thus leading to a severe underestimation of the value of CAPE. The buoyancy is evaluated using virtual temperatures for the parcel and the environment in all cases.

Listing 1: Evaluation of CAPE (CIN) and a representation of a sounding

```
data(RadiosondeDavenport)
dPs<-RadiosondeDavenport[,1]*100
dTs<-C2K(RadiosondeDavenport[,3])
dws<-RadiosondeDavenport[,6]/1000
# Dew point T in Celsius for plotting
dTd<-RadiosondeDavenport[,4]
# Initial conditions are known.
# upToTop<-FALSE "stop after the parcel is not buoyant"
capeOut<-CAPE_CIN(Ps=dPs,Ts=dTs,ws=dws,deltaP=1,
          P0=97500,T0=300.6,w0=0.01936,upToTop=FALSE,
          getLiftedBack=FALSE,precoolType="none")
```

```
# some of the information from the output object
print(paste("Davenport_CAPE:",capeOut$cape,
        "J/kg","CIN:",capeOut$cin,"J/kg","LFC",
        capeOut$apLFC$P,"Pa",capeOut$apLFC$Temp,"K"))
# Whole sounding (upToTop<-TRUE), parcel is returned
capeOut<-CAPE_CIN(Ps=dPs,Ts=dTs,ws=dws,deltaP=1,
        P0=97500,T0=300.6,w0=0.01936,
        upToTop=TRUE, getLiftedBack=TRUE)
# Plot sounding
plot<-stuve_diagram(Pres=dPs/100,Temp=K2C(dTs))
# Dew point temperature
lines(dTd,dPs/100,col="magenta",lwd=2)
# Lifted parcel (upToTop=TRUE)
lines(K2C(capeOut$Tl),(capeOut$Pl/100),
        col="black",lwd=2,lty=2)
```

A profiler has been used to evaluate the CPU time that *aiRthermo* requires to calculate saturated adiabatic evolution from an initial pressure of 950 hPa to 200 hPa (pressure step of 1 Pa). A routine that performs the same computation using an R iteration was also written. The evolution takes 50 ms using *aiRthermo*, however, that using R alone takes approximately 1500 ms. Therefore, the speed is approximately thirty times faster due to the use of the C core for computing vertical evolutions.

5. Case study: Instability indices over the Iberian Peninsula (2010-2014)

The performance of the package has been checked using a large number of real soundings measured over the Iberian Peninsula (Figure 1), an area well known for the development of convective systems [22].

In this case study, 24072 soundings from the eight stations were processed to estimate the performance of the package using realistic data. CAPE and CIN were computed using a very low vertical step (0.5 Pa), and all the soundings extended to the top of the sounding. CAPE and CIN were computed twice for two different initial parcels (one from the lowest point of the sounding, and the second from a low-level average). The K, Total-Totals, Lifted, and Showalter indices were also computed. This process took six hours on a common desktop computer (2015) running Linux.

The results of CAPE computed by *aiRthermo* and the value stored at the University of Wyoming server were compared. Figure 4 shows the resulting scatterplots for A Coruña (Atlantic site) and Barcelona (Mediterranean). The Pearson's correlation coefficient R value is very good in both cases, at 0.94 in A Coruña (3521 soundings) and 0.98 in Barcelona (3575 soundings). The values of R were within a range of $[0.94, 0.99]$ at all stations.

As shown in Figure 4, there are some clear outliers in the scatterplots. An analysis comparing some of these points (tagged with numbers) that yield different CAPE values to those provided by Wyoming has been conducted. In the first case (Barcelona, May 8th, 2011), *aiRthermo* computes a CAPE of 2625 J/kg, while Wyoming computes a CAPE of 1155 J/kg. This difference is due to the sensitivity to the initial conditions that characterise the CAPE value. We cannot be certain of the manner in which the vertical evolutions are initialised in the Wyoming server, but we have verified that errors smaller than 2% in the estimation of the initial state of the parcel (its pressure or temperature) lead to differences of 100% between the resulting CAPE values of this sounding, characterised by almost complete saturation until 500 hPa. The second case (Barcelona, August 26th, 2012) corresponds to a sounding with no moisture in the mixing ratio column of the Wyoming archive beyond 700 hPa. As the data are missing, aiRthermo is forced to stop at that level because there is no moisture information in the mixing ratio column. If the mixing ratio is assumed to be zero beyond that point and the whole sounding is processed, the differences are small (1767 J/kg in *aiRthermo* vs 1651 J/kg in Wyoming). Finally, the third analysed example corresponds to A Coruña, 27th June 2012. In this case, the mixing ratio column in the table distributed by Wyoming contains zeros. However, the moisture is not completely missing. A value of CAPE similar to that on Wyoming's web page (1247 J/kg) is computed by *aiRthermo* (1211 J/kg) if the moisture is computed from the dew point temperature in Wyoming's server.

Although the exact initial conditions used for computing CAPE in Wyoming

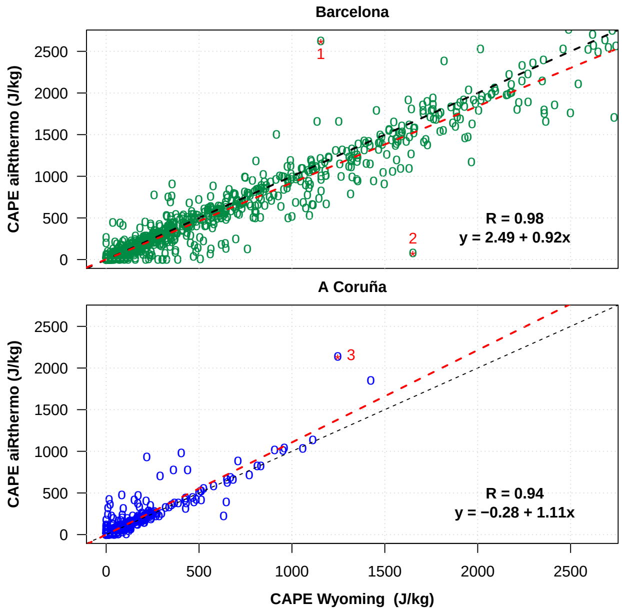

Figure 4: Scatterplot of the CAPE values computed by *aiRthermo* and the corresponding values computed by the University of Wyoming for Barcelona (top) and A Coruña (bottom).

are unknown to us, which means that the sensitivity of the results caused by this cannot be fully evaluated, the least squares regression lines exhibit high agreement, with slopes very close to one (0.92 and 1.11, as shown in Figure 4).

6. Discussion and Conclusions

This paper presents a new package for R, *aiRthermo*, which is available in the open-source repository for R packages CRAN. It provides R with new functions in the field of atmospheric thermodynamics. These capabilities considerably extend the analyses that can be conducted from inside the R interpreter.

In the field of storm forecasting, the parameters that can be computed using *aiRthermo* have been used to forecast storms in Belgrado [23]. Therefore, the ability to run different statistical models and verification procedures from inside R alongside computing the indices themselves could boost this type of study. Similar analysis [24] has been conducted in the Arctic region (Bjørnøya, Jan Mayen and Svalbard Islands), and the results of the distribution of instability indices were very different to those of other European regions [25]. The instability indices available in *aiRthermo* have been combined with satellite data from regional instability indices in Africa [26] and India [27]. These results show that analysing the climatological distribution of atmospheric instability [25], its interannual variability, and its expected future distribution [22] under globally changing conditions can benefit from using *aiRthermo*. As some instability indices must be computed from vertical adiabatic evolutions of air parcels close to the surface (the case of CAPE or LI), analysing these distributions is easier if every sounding can be processed in a much shorter time (as performed by *aiRthermo*). This will increase the use of instability indices in downscaling methods that are designed to operate on daily precipitation [28], even for long periods of time.

As well as precipitation forecasts, other damaging effects can be derived from atmospheric convective instability. Atmospheric instability indices are used to analyse lightning in Western Patagonia [29] and the Iberian Peninsula [30]. They also serve as prognostic variables when statistically downscaling wind variability [31]. The aircraft safety field is another area where the thermodynamic properties of air, particularly when it is close to saturation, are important, both at the surface, during the prevention of fog (when studying ice fog, for example [32]), or aloft to prevent the aircraft from icing [33].

The authors have also recently used the package for educational purposes in the case of M.Sc. studies in the University of Basque Country [34]. Students use the routines in the package to numerically simulate the vertical evolution of parcels and verifying their results with those they obtain from thermodynamic diagrams. They also assess the role of large-scale moisture convergence against convection in intense precipitation events by computing instability indices for air parcels, and solve simple exercises related to the Föhn effect [13].

There is a perpetual need for verifying complex forecasting systems based on advanced numerical models. The diagnostics available in *aiRthermo* are often used in these verification processes [35]. The direct availability of these diagnostics from the package used for the verification (frequently R itself) will quicken the development of these models. This also includes new satellite systems, such as GOES-R [36, 37], which can produce integrated instability indices, such as LI, almost in real-time. The ability to easily compute the values of LI, CAPE, or other indices from soundings, satellite sounders [38, 39], and numerical model results will increase the ease of the interoperability of modelled and observational data (soundings, satellite-derived products, and remotely sensed information) in newly developed operational environmental forecasting systems.

7. Acknowledgements

The authors acknowledge funding from project CGL2016-76561-R of the Spanish National Research project (MINECO and FEDER, UE). SJGR is supported by a FPI postdoctoral research grant (MINECO BES-2014-069977). Additional funding was provided by EOLO GIU17/02 (University of Basque Country, UPV/EHU). The upper air reports provided by the server run by the University of Wyoming, Dept. of Atmospheric Science, are greatly acknowledged. Constructive comments by two anonymous reviewers and the editor have improved our manuscript.

8. Software and data availability

The software presented in this paper is a package prepared to work within the R data analysis suite and was developed by the authors:

- Jon Sáenz
- Santos J. González-Rojí.
- Sheila Carreno-Madinabeitia
- Gabriel Ibarra-Berastegi

Contact address: Jon Sáenz, Dept. of Applied Physics II, Faculty of Science and Technology, UPV/EHU, Barrio Sarriena s/n, 48940-Leioa, Spain.

Telephone: +34 946012445

Fax: +34 946013500

email addresses:

- jon.saenz@ehu.eus
- santosjose.gonzalez@ehu.eus

- sheila.carreno@tecnalia.com
- gabriel.ibarra@ehu.eus

Year first available in CRAN: 2017.

Hardware required: It has been tested on laptops, Desktops, and workstations running Mac OS, Windows, and Linux.

Availability: The software and datasets are freely available (GPL-3 license) in the Comprehensive R Archive Network (CRAN):

`https://cran.r-project.org/package=aiRthermo`

The package can be installed from any of the mirrors, which is usual for R packages, by typing `install.packages("aiRthermo")` into the R interpreter. The size of the package ranges from 400 to 500 Kb, depending on whether the source or Windows-compiled version is downloaded. The CRAN servers allow anonymous access to the package. The software is written in R and C. The manual is also provided at the CRAN server [40].

References

[1] D. C. Carslaw, K. Ropkins, openair An R package for air quality data analysis, Environmental Modelling & Software 27-28 (2012) 52–61. doi:10.1016/j.envsoft.2011.09.008.

[2] R. Serrano-Notivoli, M. de Luis, S. Beguería, An R package for daily precipitation climate series reconstruction, Environmental Modelling & Software 89 (2017) 190–195. doi:10.1016/j.envsoft.2016.11.005.

[3] J. Skøien, G. Blöschl, G. Laaha, E. Pebesma, J. Parajka, A. Viglione, rtop: An R package for interpolation of data with a variable spatial support, with an example from river networks, Computers & Geosciences 67 (2014) 180 – 190. doi:10.1016/j.cageo.2014.02.009.

[4] L. Busetto, L. Ranghetti, MODIStsp: An R package for automatic preprocessing of MODIS Land Products time series, Computers & Geosciences 97 (2016) 40 – 48. doi:10.1016/j.cageo.2016.08.020.

[5] D. Bowman, J. Lees, Near real time weather and ocean model data access with rNOMADS, Computers & Geosciences 78 (2015) 88 – 95. doi:10.1016/j.cageo.2015.02.013.

[6] C. F. Bohren, B. A. Albrecht, Atmospheric Thermodynamics, Oxford University Press, New York, 1998.

[7] G. W. Petty, A First Course in Atmospheric Thermodynamics, Sundog Publishing, Madison, 2008.

[8] G. R. North, T. L. Erukhimova, Atmospheric Thermodynamics, Cambridge University Press, New York, 2009.

[9] Z. Liang, D. Wang, Sea breeze and precipitation over Hainan Island, Quarterly Journal of the Royal Meteorological Society 143 (2017) 137–151. doi:10.1002/qj.2952.

[10] C. A. Doswell III, H. E. Brooks, R. A. Maddox, Flash flood forecasting: An ingredients-based methodology, Weather and Forecasting 11 (1996) 560–581. doi:10.1175/1520-0434(1996)011<0560:FFFAIB>2.0.CO;2.

[11] V. Petković, C. D. Kummerow, Understanding the sources of satellite passive microwave rainfall retrieval systematic errors over land, Journal of Applied Meteorology and Climatology 56 (2017) 597–614. doi:10.1175/JAMC-D-16-0174.1.

[12] G. Ibarra-Berastegi, J. Sáenz, A. Ezcurra, A. Elías, J. Díaz de Argandoña, I. Errasti, Downscaling of surface moisture flux and precipitation in the Ebro Valley (Spain) using analogues and analogues followed by random forests and multiple linear regression, Hydrology and Earth System Sciences 15 (2011) 1895–1907. doi:10.5194/hess-15-1895-2011.

[13] J. Sáenz, S. González-Rojí, S. Carreno-Madinabeitia, G. Ibarra-Berastegi, Airthermo: An R package designed to help students understanding atmospheric thermodynamics, in: EDULEARN18 Proceedings, 10th International Conference on Education and New Learning Technologies, IATED, 2018, pp. 1567–1573.

[14] A. A. Tsonis, An Introduction to Atmospheric Thermodynamics, Cambridge University Press, Cambridge, 2002.

[15] R. R. Rogers, M. K. Yau, A Short Course in Cloud Physics, 3rd Edition, Pergamon Press, Oxford, 1989.

[16] A. L. Buck, New equations for computing vapor pressure and enhancement factor, Journal of Applied Meteorology 20 (1981) 1527–1532. doi:10.1175/1520-0450(1981)020<1527:NEFCVP>2.0.CO;2.

[17] R. Feistel, W. Wagner, A new equation of state for H2O ice Ih, Journal of Physical and Chemical Reference Data 35 (2006) 1021–1047. doi:10.1063/1.2183324.

[18] J. P. Craven, R. E. Jewell, H. E. Brooks, Comparison between observed convective cloud-base heights and lifting condensation level for two different lifted parcels, Weather and Forecasting 17 (2002) 885–890. doi:10.1175/1520-0434(2002)017<0885:CBOCCB>2.0.CO;2.

[19] C. E. Letkewicz, M. D. Parker, Forecasting the maintenance of mesoscale convective systems crossing the Appalachian Mountains, Weather and Forecasting 25 (2010) 1179–1195. doi:10.1175/2010WAF2222379.1.

[20] C. A. Doswell III, E. N. Rasmussen, The effect of neglecting the virtual temperature correction on CAPE calculations, Weather and Forecasting 9 (1994) 625–629. doi:10.1175/1520-0434(1994)009<0625:TEONTV>2.0.CO;2.

[21] D. Bolton, The computation of equivalent potential temperature, Monthly Weather Review 108 (1980) 1046–1053. doi:10.1175/1520-0493(1980)108<1046:TCOEPT>2.0.CO;2.

[22] C. Viceto, M. Marta-Almeida, A. Rocha, Future climate change of stability indices for the Iberian Peninsula, International Journal of Climatology n/a (2017) 4390–4408. doi:10.1002/joc.5094.

[23] D. Vujović, M. Paskota, N. Todorović, V. Vučković, Evaluation of the stability indices for the thunderstorm forecasting in the region of belgrade,

serbia, Atmospheric Research 161 (2015) 143 – 152. doi:10.1016/j.atmosres.2015.04.005.

[24] B. Czernecki, M. Taszarek, L. Kolendowicz, K. Szyga-Pluta, Atmospheric conditions of thunderstorms in the European part of the Arctic derived from sounding and reanalysis data, Atmospheric Research 154 (2015) 60 – 72. doi:10.1016/j.atmosres.2014.11.001.

[25] M. Siedlecki, Selected instability indices in Europe, Theoretical and Applied Climatology 96 (2009) 85–94. doi:10.1007/s00704-008-0034-4.

[26] E. de Coning, M. Koenig, J. Olivier, The combined instability index: a new very-short range convection forecasting technique for southern Africa, Meteorological Applications 18 (2011) 421–439. doi:10.1002/met.234.

[27] S. Chaudhuri, J. Pal, A. Middey, S. Goswami, Nowcasting Bordoichila with a composite stability index, Natural Hazards 66 (2013) 591–607. doi:10.1007/s11069-012-0504-y.

[28] T. Iizumi, M. Nishimori, K. Dairaku, S. A. Adachi, M. Yokozawa, Evaluation and intercomparison of downscaled daily precipitation indices over Japan in present-day climate: Strengths and weaknesses of dynamical and bias correction-type statistical downscaling methods, Journal of Geophysical Research: Atmospheres 116 (D1) (2011) D01111. doi:10.1029/2010JD014513.

[29] R. D. Garreaud, M. G. Nicora, R. E. Bürgesser, E. E. Ávila, Lightning in Western Patagonia, Journal of Geophysical Research: Atmospheres 119 (2014) 4471–4485. doi:10.1002/2013JD021160.

[30] J. A. Santos, M. A. Reis, F. De Pablo, L. Rivas-Soriano, S. M. Leite, Forcing factors of cloud-to-ground lightning over Iberia: regional-scale assessments, Natural Hazards and Earth System Sciences 13 (7) (2013) 1745–1758. doi:10.5194/nhess-13-1745-2013.

[31] R. J. Davy, M. J. Woods, C. J. Russell, P. A. Coppin, Statistical downscaling of wind variability from meteorological fields, Boundary-Layer Meteorology 135 (2010) 161–175. doi:10.1007/s10546-009-9462-7.

[32] I. Gultepe, B. Zhou, J. Milbrandt, A. Bott, Y. Li, A. Heymsfield, B. Ferrier, R. Ware, M. Pavolonis, T. Kuhn, J. Gurka, P. Liu, J. Cermak, A review on ice fog measurements and modeling, Atmospheric Research 151 (2015) 2 – 19. doi:10.1016/j.atmosres.2014.04.014.

[33] B. C. Bernstein, C. A. Wolff, F. McDonough, An inferred climatology of icing conditions aloft, including supercooled large drops. Part I: Canada and the continental United States, Journal of Applied Meteorology and Climatology 46 (2007) 1857–1878. doi:10.1175/2007JAMC1607.1.

[34] A. Sánchez-Lavega, S. Pérez-Hoyos, R. Hueso, T. del Río-Gaztelurrutia, A. Oleaga, The Aula EspaZio Gela and the Master of Space Science and Technology in the Universidad del País Vasco (University of the Basque Country), European Journal of Engineering Education 39 (2014) 518–526. doi:10.1080/03043797.2013.788611.

[35] T. A. Jones, S. Koch, Z. Li, Assimilating synthetic hyperspectral sounder temperature and humidity retrievals to improve severe weather forecasts, Atmospheric Research 186 (2017) 9 – 25. doi:10.1016/j.atmosres.2016.11.004.

[36] T. J. Schmit, J. Li, J. Li, W. F. Feltz, J. J. Gurka, M. D. Goldberg, K. J. Schrab, The GOES-R advanced baseline imager and the continuation of current sounder products, Journal of Applied Meteorology and Climatology 47 (2008) 2696–2711. doi:10.1175/2008JAMC1858.1.

[37] T. J. Schmit, J. Li, S. A. Ackerman, J. J. Gurka, High-spectral- and high-temporal-resolution infrared measurements from geostationary orbit, Journal of Atmospheric and Oceanic Technology 26 (2009) 2273–2292. doi:10.1175/2009JTECHA1248.1.

[38] S. J. Lee, M.-H. Ahn, Y. Lee, Application of an artificial neural network for a direct estimation of atmospheric instability from a next-generation imager, Advances in Atmospheric Sciences 33 (2016) 221–232. doi:10.1007/s00376-015-5084-9.

[39] T. J. Schmit, P. Griffith, M. M. Gunshor, J. M. Daniels, S. J. Goodman, W. J. Lebair, A closer look at the ABI on the GOES-R series, Bulletin

of the American Meteorological Society 98 (2017) 681–698. doi:10.1175/BAMS-D-15-00230.1.

[40] J. Sáenz, S. J. González-Rojí, S. Carreno-Madinabeitia, G. Ibarra-Berastegi, aiRthermo: Atmospheric Thermodynamics and Visualization, r package version 1.2 (2018).
URL https://CRAN.R-project.org/package=aiRthermo